Proceedings of the IASS 2024 Symposium
Redefining the Art of Structural Design
August 26-30, 2024, Zurich, Switzerland
Philippe Block, Giulia Boller, Catherine DeWolf,
Jacqueline Pauli, Walter Kaufmann (eds.)

Topology optimization of deployable structures using ground structures generated by tessellation of origami tubes

Sunao TOMITA[a], Hiroki KOBAYASHI[a], Shoko ARITA[a], Masato TANAKA[a], Atsushi KAWAMOTO[a], Tsuyoshi NOMURA[a],Tomohiro TACHI*

* The University of Tokyo
3-8-1 Komaba, Meguro-Ku, Tokyo, Japan
tachi@idea.c.u-tokyo.ac.jp

[a] Toyota Central R&D Labs., Inc., 1-4-14 Koraku, Bunkyo-ku, Tokyo 112-0004, Japan

Abstract

Deployable structures can be transformed from a compact state to a deployed configuration, which enhances the transportability and rapid construction of structures such as transitional shelters. The design of deployable structures requires assessing soft deployment motion, high stiffness after deployment, and lightweightness. To satisfy these requirements, origami-based structures play a vital role because coupling origami tubes provides extremely high stiffness and assures developability. To apply the features of origami-based structures for foldable structures under various load conditions, the design framework to determine the optimal connectivity of origami panels must be established. Toward this end, this study performs topology optimization on the ground structures generated by the origami tessellations to minimize the objective function. Among the origami tessellations, three-dimensional tessellation of Miura-ori tubes, referred to as interleaved cellular origami structures, is employed because the tessellation provides rigid foldability after thickness accommodation and high stiffness by the coupling effect. Therefore, the ground structures based on the tessellation enable us to easily handle the valid mechanisms using thick panels and keep the high stiffness during deployment. This study performs the topology optimization by density approach. The ground structures based on Miura-ori tubes are discretized by bar-and-hinge models, where the folding and bending of panels are represented by rotational springs, and the stretching of panels is expressed by bar elements. To ensure the connectivity of panels as the Miura-ori tubes, the densities on panels are calculated by projecting design variables on nodes using the projection function that averages the weighted design variables on a neighborhood specified by a circle with the filter radius. Furthermore, the density functions are computed by the Heaviside function to obtain the valid configuration of Miura-ori tubes. Numerical examples of compliance minimization demonstrate the design of the optimal connectivity of the Miura-ori tubes for lightweight deployable structures.

Keywords: Miura-ori, origami tessellation, mechanism, bar-and-hinge model, topology optimization, ground structure

1. Introduction

The construction of deployable structures offers several benefits, including rapid assembly and high transportability due to their compact nature. Among deployable structures, rigid origami, in which rigid panels are connected via creases, has a significant advantage in realizing folding and deployment motions. Because programmable motions by folding are scalable, rigid origami has potential applications

at various scales, from the deployment of solar sails in space [1] to the construction of shelters [2, 3], arches [4], and medical stents [5].

The concept of coupling origami tubes to make cellular materials has been explored to achieve distinctive mechanical properties. Previous studies have introduced origami metamaterials with negative Poisson's ratios [6]. Additionally, highly stiff deployable structures, known as zipper-coupled tubes [7], have been proposed based on the Miura ori. Thick Miura-ori tubes have also been connected along their creases, resulting in stiffness comparable to zipper coupling [8]. Tachi-Miura polyhedra are also composed of origami tubes [9], which lead to auxeticity [10], load-bearing capability [11], and high-efficiency energy absorption [12, 13, 14]. To enhance the performance of these origami-based cellular structures, the design frameworks to determine the connectivity of the units in the origami tessellation are necessary.

Topology optimization [15] has been employed in structural engineering to design the layout and connectivity of the element. Topology optimization of deployable or foldable structures has been investigated, e.g., crease pattern design of origami based on the ground structure approach [16, 17], foldable structures made of piecewise developable surfaces [18], and the scissor-type structures [19]. By contrast, to our best knowledge, the design strategy to determine the optimum connectivity of the cellular origami tessellation has not been established.

This study presents the topology optimization using the ground structures based on interleaved cellular origami structures [20]. We employ interleaved cellular origami structures because they can be realized as thick origami and have high stiffness [21]. The geometry is discretized by bar-and-hinge models, which represent the folding and bending of panels by rotational springs and the stretching of panels by bar elements. To ensure the connectivity of panels as the Miura-ori tubes, the densities on panels are calculated by the projection of design variables on nodes using the projection function that averages the weighted design variables on a neighborhood specified by a circle with the filter radius. Furthermore, the density functions are computed by the Heaviside function to obtain the valid configuration of Miura-ori tubes. Numerical examples of compliance minimization demonstrate the design of the optimal connectivity of the Miura-ori tubes for lightweight deployable structures.

2. Geometry of origami tessellation

2.1. Miura-ori tube

Dimension of Miura-ori unit cell is defined as shown in Fig. 1 (a). Length of Miura-ori a, b, the internal angle of the parallelogram α and dihedral folding angle $\theta \in [0, \pi/2]$ provide one-degree-of-freedom motions. The dimensions of unit cells are defined as:

$$L_x = 2b\frac{\cos\theta\tan\alpha}{\sqrt{1+\cos^2\theta\tan^2\alpha}} \tag{1}$$

$$L_y = 2a\sqrt{1-\sin^2\theta\sin^2\alpha}, \tag{2}$$

$$H = 2a\sin\theta\sin\alpha, \tag{3}$$

and

$$V = b\frac{1}{\sqrt{1+\cos^2\theta\tan^2\alpha}}. \tag{4}$$

The Miura-ori tubes are created by coupling Miura-ori to that mirrored along x-y plane as shown in Fig. 1 (b).

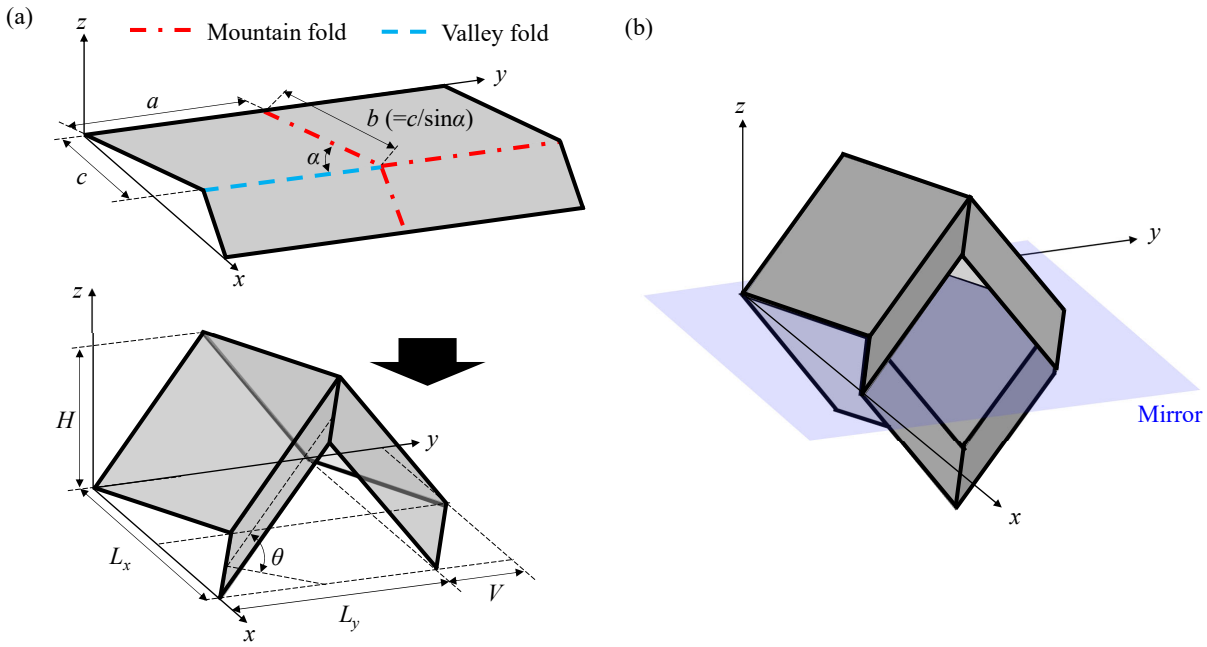

Figure 1: Geometry of Miura-ori tube (a) Unit cell of Miura-ori sheet (b) Miura-ori tube created by coupling mirrored Miura-ori sheet.

2.2. Tessellated structure

The coupling of the 180°-rotated Miura-ori tubes along the creases leads to tessellation in the 3D space, as shown in Fig. 2. The resulting cellular structures could rigidly deform from one flat state to another because all interfaces for coupling thick Miura-ori tubes maintain local mirror symmetry. This tessellation of thick Miura-ori tubes results in thickness accommodation of the interleaved cellular origami structures proposed in [20]. Also, these cellular structures have high stiffness through the development [21], which is similar to zipper coupling [7]. Therefore, we employ this tessellation as the ground structure to ensure rigid foldability and easy fabrication.

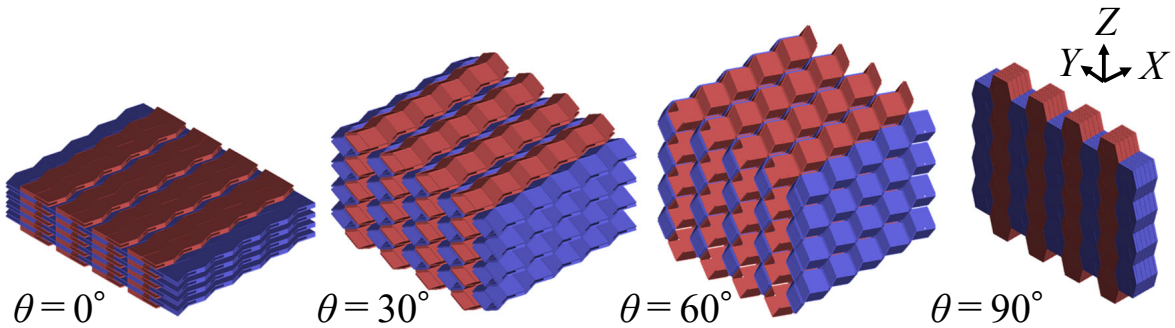

Figure 2: Coupling of the 180°-rotated Miura-ori tubes along creases.

3. Formulation

3.1. Bar-and-hinge model

Ground structures generated by tessellation of Miura-ori tubes are discretized by bar-and-hinge models [22], where the displacement $\mathbf{u}$ are represented by the extension of bar element $\mathbf{e}$, the bending angle of

panels and folding Θ_B and Θ_F as:

$$\begin{pmatrix} \mathbf{C} \\ \mathbf{J}_B \\ \mathbf{J}_F \end{pmatrix} \mathbf{u} = \begin{pmatrix} \mathbf{e} \\ \boldsymbol{\Theta}_B \\ \boldsymbol{\Theta}_F \end{pmatrix}, \tag{5}$$

where $\mathbf{C}$, $\mathbf{J}_B$ and $\mathbf{J}_F$ are compatibility matrices, respectively. Furthermore, linear elastic constitutive law is:

$$\begin{pmatrix} \mathbf{K}_S & \mathbf{0} & \mathbf{0} \\ \mathbf{0} & \mathbf{K}_B & \mathbf{0} \\ \mathbf{0} & \mathbf{0} & \mathbf{K}_F \end{pmatrix} \begin{pmatrix} \mathbf{e} \\ \boldsymbol{\Theta}_B \\ \boldsymbol{\Theta}_F \end{pmatrix} = \begin{pmatrix} \mathbf{t} \\ \mathbf{m}_B \\ \mathbf{m}_F \end{pmatrix}, \tag{6}$$

where $\mathbf{K}_S$, $\mathbf{K}_B$ and $\mathbf{K}_F$ are diagonal matrices represented by stretch and shear deformation of panels characterized by bar elements, bending of panels characterized by hinge elements on the diagonals of panels and the bending stiffness of creases characterized by rotational spring on the creases. Furthermore, $\mathbf{t}$, $\mathbf{m}_B$ and $\mathbf{m}_F$ are the tension of bar elements, bending moment of panels and creases, respectively. In addition, the principle of virtual work provides:

$$\mathbf{f} = \mathbf{K}\mathbf{u} = \begin{pmatrix} \mathbf{C} \\ \mathbf{J}_B \\ \mathbf{J}_F \end{pmatrix}^{\mathsf{T}} \begin{pmatrix} \mathbf{e} \\ \boldsymbol{\Theta}_B \\ \boldsymbol{\Theta}_F \end{pmatrix}, \tag{7}$$

The Eqs. (5)-(7) leads to the stiffness matrix $\mathbf{K}$:

$$\mathbf{K} = \begin{pmatrix} \mathbf{C} \\ \mathbf{J}_B \\ \mathbf{J}_F \end{pmatrix}^{\mathsf{T}} \begin{pmatrix} \mathbf{K}_S & \mathbf{0} & \mathbf{0} \\ \mathbf{0} & \mathbf{K}_B & \mathbf{0} \\ \mathbf{0} & \mathbf{0} & \mathbf{K}_F \end{pmatrix} \begin{pmatrix} \mathbf{C} \\ \mathbf{J}_B \\ \mathbf{J}_F \end{pmatrix} = \mathbf{C}^{\mathsf{T}}\mathbf{K_S}\mathbf{C} + \mathbf{J_B}^{\mathsf{T}}\mathbf{K_B}\mathbf{J_B} + \mathbf{J_F}^{\mathsf{T}}\mathbf{K_F}\mathbf{J_F}, \tag{8}$$

The compatibility matrix of bar elements between nodes i and j is:

$$\mathbf{C} = \frac{1}{L}[-\mathbf{n}_{ij}, \mathbf{n}_{ij}], \tag{9}$$

where,

$$\mathbf{n}_{ij} = \frac{1}{L}(\mathbf{x}_j - \mathbf{x}_i),\ L = ||\mathbf{x}_j - \mathbf{x}_i||, \tag{10}$$

where, $\mathbf{x}$ is nodal coordinate. Furthermore, considering nodes j and k on the interface edge of two triangular planes connecting by rotational springs, other nodes on triangles i and l, compatibility of rotational spring be $\mathbf{J}$ is:

$$\mathbf{J}_i = \frac{||\mathbf{r}_{kj}||}{||\mathbf{m}_{jik}||^2}\mathbf{m}_{jik}, \tag{11}$$

$$\mathbf{J}_j = -\frac{||\mathbf{r}_{kj}||}{||\mathbf{m}_{jlk}||^2}\mathbf{m}_{jlk}, \tag{12}$$

$$\mathbf{J}_k = \left(\frac{\mathbf{r}_{ij}\cdot\mathbf{r}_{kj}}{||\mathbf{r}_{kj}||^2}\mathbf{m} - 1\right)\mathbf{J}_i - \frac{\mathbf{r}_{kl}\cdot\mathbf{r}_{kj}}{||\mathbf{r}_{kj}||^2}\mathbf{J}_j, \tag{13}$$

$$\mathbf{J}_l = \left(\frac{\mathbf{r}_{ij}\cdot\mathbf{r}_{kj}}{||\mathbf{r}_{kj}||^2}\mathbf{m} - 1\right)\mathbf{J}_j - \frac{\mathbf{r}_{ij}\cdot\mathbf{r}_{kj}}{||\mathbf{r}_{kj}||^2}\mathbf{J}_i, \tag{14}$$

where, for $p, q \in i, j, k, l$,

$$\mathbf{r}_{pq} = \mathbf{x}_p - \mathbf{x}_q, \tag{15}$$

normal vectors of triangles composed of nodes j, i, k and j, l, k are [23]:

$$\mathbf{m}_{jik} = \mathbf{r}_{ji} \times \mathbf{r}_{jk},\ \mathbf{m}_{jlk} = \mathbf{r}_{jl} \times \mathbf{r}_{jk}. \tag{16}$$

As a discretization in bar-and-hinge models, N5B8 illustrated in Fig. 3 (Panels of origami are represented by 5 nodes and 8 bars) are employed to calculate the stiffness matrix. In addition, the diagonals of the stiffness matrix $\mathbf{K}_S$, $\mathbf{K}_B$ and $\mathbf{K}_F$ [22].

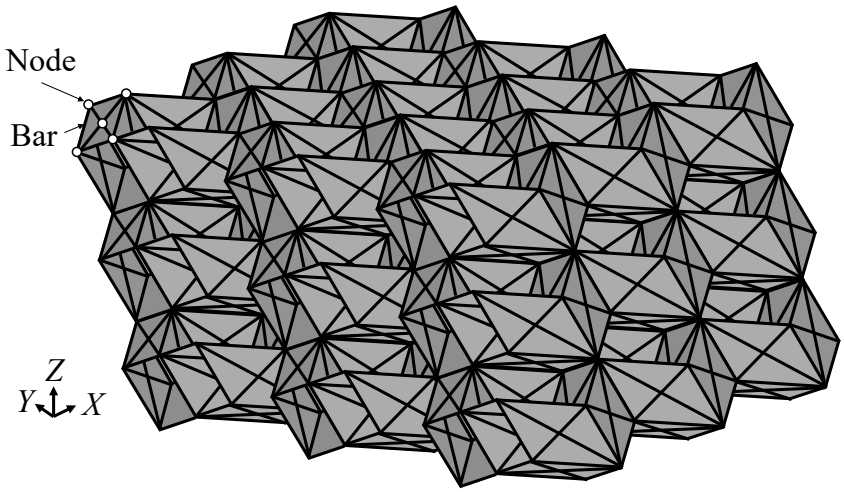

Figure 3: Schematic of bar-and-hinge model

The stiffness of bar elements to represent stretch and shear deformation are K_S (i.e., diagonals of $\mathbf{K}_S$) and thickness. K_S is:

$$K_S = EA/L, \tag{17}$$

where, E, A and L are Young's modulus and cross-sectional area and length of bars. To represent the mechanical properties of the rectangle panels by N5B8 models, the length of rectangular panels W and H, cross-sectional area of bars A_X,A_Y and A_D are:

$$A_X = t\frac{H^2 - \nu W^2}{2H(1-\nu^2)}, \tag{18}$$

$$A_Y = t\frac{W^2 - \nu H^2}{2W(1-\nu^2)}, \tag{19}$$

$$A_D = t\frac{\nu(W^2+H^2)^{3/2}}{2HW(1-\nu^2)}, \tag{20}$$

where ν and t are Poisson's ratio and thickness of panels. These relationships can empirically imitate the mechanical properties of skewed panels Miura-ori [22].

Diagonal component K_B of stiffness associated with bending of panels[22] is:

$$K_B = C_B\frac{Et^3}{12(1-\nu^2)}\left(\frac{D_S}{t}\right)^{1/3}, \tag{21}$$

where, D_S is length of short diagonal and $C_B = 1/D_S$.

3.2. Design variables

The distribution of panels in the design domain is expressed using the density $\rho_e \in [0, 1]$ associated with thickness t. According with SIMP method [15], thickness t of Miura-ori panels are:

$$t = {\rho_e}^p t_0, \tag{22}$$

where, t_0 is the thickness of the Miura-ori, p is penalty.

To avoid the checkerboard of Miura-ori panels and retain the minimum connectivity of the Miura-ori tubes, filter by [24]for design variables is introduced here. In addition, to obtain the valid geometry represented by 0 or 1, the design valuables ϕ_j on nodes of Miura-ori are calculated using the Heaviside function [25]. The design valuables on nodes of Miura-ori are filtered by: $\phi_i \in [-1, 1]$

$$\tilde{\rho}_e = \frac{\sum_{j \in S^e} \phi_j w(\mathbf{x}_j - \mathbf{x}_e)}{\sum_{j \in S^e} w(\mathbf{x}_j - \mathbf{x}_e)}, \tag{23}$$

where, S^e is set of nodes in the cube with radius R_{min} with node center $\mathbf{x}_e$, w is weight function:

$$w(\mathbf{x}_j - \mathbf{x}_e) = \begin{cases} \frac{R_{min} - ||\mathbf{x}_j - \mathbf{x}_e||}{R_{\min}} & \text{if } \mathbf{x_e} \in \Omega_e, \\ \mathbf{0} & \text{otherwise} \end{cases} \tag{24}$$

The density $\tilde{\rho}_e$ is calculated by using Heaviside function:

$$\rho_e = \frac{\tanh(\beta \tilde{\rho}_e)}{2 \tanh(\beta)} + 0.5. \tag{25}$$

3.3. Optimization problem

This study deals with the minimizing compliance defined as:

$$\min : c(\rho_1, \ldots, \rho_N) \coloneqq \mathbf{U}^\top \mathbf{K} \mathbf{U} \tag{26}$$

$$\text{subject to: } \mathbf{K}\mathbf{U} = \mathbf{F} \tag{27}$$

$$\sum_{e=1}^{N} \rho_e / N < V_f \tag{28}$$

$$0 < \rho^{min} < \rho_e < 1 \tag{29}$$

where V_f is the volume fraction of panels on the ground structures and N is the number of panels in the ground structure. Stiffness matrix $\mathbf{K}$ and displacement vector $\mathbf{U}$ are assembled as:

$$\mathbf{U}^\top \mathbf{K} \mathbf{U} = \sum_{e=1}^{N} \mathbf{u}_{Se}^\top \mathbf{k}_{Se} \mathbf{u}_{Se} + \sum_{e=1}^{N} \mathbf{u}_{Be}^\top \mathbf{k}_{Be} \mathbf{u}_{Be}, \tag{30}$$

Using density ρ_e, the local stiffness matrix associated with in-plane deformation is

$$\mathbf{k}_{Se} = \rho_e^p \mathbf{k}_{S0}, \tag{31}$$

the local stiffness matrix associated with out-of-plane deformation is

$$\mathbf{k}_{Be} = \rho_e^{(8/3)p} \mathbf{k}_{B0}. \tag{32}$$

The optimization problem was solved by the Method of Moving Asymptotes [26].

3.4. Sensitivity analysis

The sensitivity of the objective function c with independent design variables ϕ_j is defined from the chain rule:

$$\frac{\partial c}{\partial \phi_j} = \frac{\partial c}{\partial \rho_e}\frac{\partial \rho_e}{\partial \tilde{\rho}_e}\frac{\partial \tilde{\rho}_e}{\partial \phi_j}, \tag{33}$$

where

$$\frac{\partial c}{\partial \rho_e} = -p(x_e)^{p-1}\mathbf{u}_e^\top \mathbf{k}_{S0}\mathbf{u}_e - \frac{8}{3}p(x_e)^{\frac{8}{3}p-1}\mathbf{u}_e^\top \mathbf{k}_{B0}\mathbf{u}_e, \tag{34}$$

$$\frac{\partial \rho_e}{\partial \tilde{\rho}_e} = \frac{\beta\,\mathrm{sech}^2(\beta\tilde{\rho}_e)}{2\tanh(\beta)}, \tag{35}$$

and

$$\frac{\partial \tilde{\rho}_e}{\partial \phi_j} = \frac{w(\mathbf{x}_j - \mathbf{x}_e)}{\sum_{j\in S^e} w(\mathbf{x}_j - \mathbf{x}_e)}. \tag{36}$$

4. Result

The geometry of the unit cell is defined by parameters $a = c = 1$, $\alpha = 55^o$. Young's modulus, density, Poisson's ratio, and thickness of panels are 10^6, 1, 1/3, 0.01 used in [7], respectively. The scaling factor of stiffness of hinges along creases is set as 40 used in [22]. Ground structures were created by tessellation of the 180°-rotated Miura-ori tubes shown in Fig. 4 under the $\theta = 60°$ folded states, where 1, 6.5 and 5.5 units in direction x-, y- and z-axis are used. The load was applied on the left edge shown in Fig. 4 and the right edge was fixed. The penalty $p = 3$, the radius of filter $R_{min} = 3$, and volume fraction $V_f = 0.6$ are employed. The black panels shown in Fig. 4 were obtained by optimization. Owing to the one-DOF motions of the tessellated structures, the optimum structures have the flat foldability shown in Fig. 5.

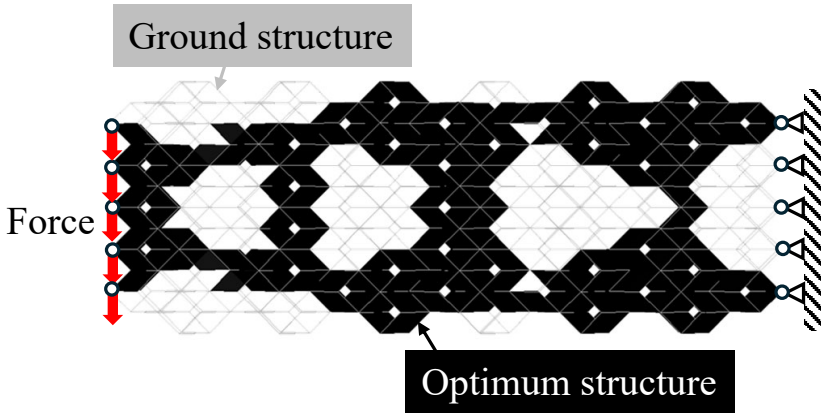

Figure 4: Numerical examples of the topology optimization to determine the connectivity of the Miura-ori tubes.

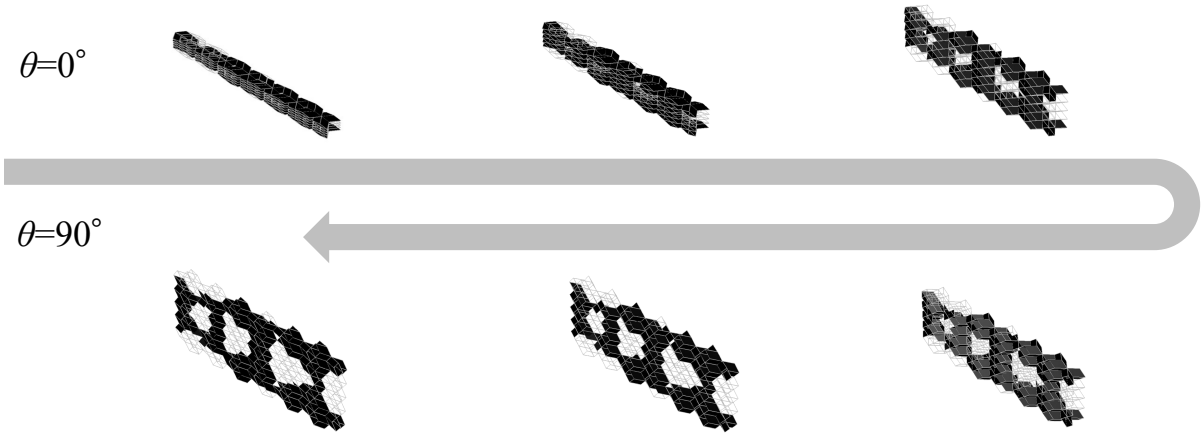

Figure 5: Folding of the optimized structure by one-DOF motions of tessellated Miura-ori tubes.

5. Conclusion

This study introduced the topology optimization using foldable ground structures to design the deployable structures. The ground structures were defined by tessellation of 180°-rotated Miura-ori tubes, which eases the connection of thick Miura-ori tubes. The connectivity of the Miura-ori tubes was optimized by minimizing compliance using the sensitivity with respect to the panel thickness based on the bar-and-hinge models. To ensure the connectivity of panels as cellular structures, the densities on panels were calculated by projecting design variables on nodes using the projection function that averages the weighted design variables on a neighborhood specified by a circle with the filter radius. Furthermore, the density functions were computed by the Heaviside function to obtain the valid configuration of Miura-ori tubes. Numerical examples of compliance minimization demonstrate the design of the optimal connectivity of the Miura-ori tubes, which enables the construction of lightweight structures by connecting the deployable units based on Miura-ori tubes. The proposed design framework will be applied to the design of three-dimensional structures. In addition, the fabrication of the optimum structures using thick panels and their evaluation will be performed to demonstrate the stability and durability of the structures.

References

[1] K. Miura, "Method of packaging and deployment of large membranes in space," *The Institute of Space and Astronautical Science report*, vol. 618, pp. 1–9, 1985.

[2] D. Melancon, B. Gorissen, C. J. García-Mora, C. Hoberman, and K. Bertoldi, "Multistable inflatable origami structures at the metre scale," *Nature*, vol. 592, no. 7855, pp. 545–550, 2021. DOI: 10.1038/s41586-021-03407-4.

[3] J. M. Gattas and Z. You, "Geometric assembly of rigid-foldable morphing sandwich structures," *Engineering Structures*, vol. 94, pp. 149–159, 2015. DOI: 10.1016/j.engstruct.2015.03.019.

[4] J. M. Gattas, W. Lv, and Y. Chen, "Rigid-foldable tubular arches," *Engineering Structures*, vol. 145, pp. 246–253, 2017. DOI: 10.1016/j.engstruct.2017.04.037.

[5] K. Kuribayashi *et al.*, "Self-deployable origami stent grafts as a biomedical application of ni-rich tini shape memory alloy foil," *Materials Science and Engineering: A*, vol. 419, no. 1, pp. 131–137, 2006. DOI: 10.1016/j.msea.2005.12.016.

[6] M. Schenk and S. D. Guest, "Geometry of miura-folded metamaterials," *Proceedings of the National Academy of Sciences*, vol. 110, no. 9, pp. 3276–3281, 2013. DOI: 10.1073/pnas.1217998110.

[7] E. T. Filipov, T. Tachi, and G. H. Paulino, "Origami tubes assembled into stiff, yet reconfigurable structures and metamaterials," *Proceedings of the National Academy of Sciences*, vol. 112, no. 40, pp. 12 321–12 326, 2015. DOI: 10.1073/pnas.1509465112.

[8] S. Tomita, K. Shimanuki, K. Umemoto, A. Kawamoto, T. Nomura, and T. Tachi, "Coupled thick-panel origami tubes along creases for stiff deployable structures," *Proceedings of IASS Annual Symposia*, vol. 2023, no. 19, pp. 1–9, 2023.

[9] T. Tachi and K. Miura, "Rigid-foldable cylinders and cells," *Journal of the International Association for Shell and Spatial Structures*, vol. 53, no. 4, pp. 217–226, 2012.

[10] H. Yasuda and J. Yang, "Reentrant origami-based metamaterials with negative poisson's ratio and bistability," *Physical Review Letters*, vol. 114, no. 18, p. 185 502, 2015. DOI: 10.1103/PhysRevLett.114.185502.

[11] H. Yasuda, B. Gopalarethinam, T. Kunimine, T. Tachi, and J. Yang, "Origami-based cellular structures with in situ transition between collapsible and load-bearing configurations," *Advanced Engineering Materials*, vol. 21, no. 12, p. 1 900 562, 2019. DOI: 10.1002/adem.201900562.

[12] S. Tomita *et al.*, "Origami-inspired metamaterials with switchable energy absorption based on bifurcated motions of a tachi-miura polyhedron," *Materials & Design*, vol. 225, p. 111 497, 2023. DOI: 10.1016/j.matdes.2022.111497.

[13] S. Tomita *et al.*, "Transition of deformation modes from bending to auxetic compression in origami-based metamaterials for head protection from impact," *Scientific Reports*, vol. 13, no. 1, p. 12 221, 2023. DOI: 10.1038/s41598-023-39200-8.

[14] S. Tomita, K. Shimanuki, and K. Umemoto, "Control of buckling behavior in origami-based auxetic structures by functionally graded thickness," *Journal of Applied Physics*, vol. 135, no. 10, 2024. DOI: 10.1063/5.0194238.

[15] M. P. Bendsøe and N. Kikuchi, "Generating optimal topologies in structural design using a homogenization method," *Computer Methods in Applied Mechanics and Engineering*, vol. 71, no. 2, pp. 197–224, 1988. DOI: 10.1016/0045-7825(88)90086-2.

[16] K. Fuchi *et al.*, "Origami actuator design and networking through crease topology optimization," *Journal of Mechanical Design*, vol. 137, no. 9, 2015. DOI: 10.1115/1.4030876.

[17] A. S. Gillman, K. Fuchi, and P. R. Buskohl, "Discovering sequenced origami folding through nonlinear mechanics and topology optimization," *Journal of Mechanical Design*, vol. 141, no. 4, 2019. DOI: 10.1115/1.4041782.

[18] Y. Zhou, T. Nomura, E. M. Dede, and K. Saitou, "Topology optimization with wall thickness and piecewise developability constraints for foldable shape-changing structures," *Structural and Multidisciplinary Optimization*, vol. 65, no. 4, p. 118, 2022. DOI: 10.1007/s00158-022-03219-8.

[19] L. I. W. Arnouts, T. J. Massart, N. De Temmerman, and P. Z. Berke, "Coupled sizing, shape and topology optimisation of bistable deployable structures," *Journal of the International Association for Shell and Spatial Structures*, vol. 61, no. 4, pp. 264–274, 2020. DOI: 10.20898/j.iass.2020.009.

[20] K. C. Cheung, T. Tachi, S. Calisch, and K. Miura, "Origami interleaved tube cellular materials," *Smart Materials and Structures*, vol. 23, no. 9, p. 094 012, 2014. DOI: 10.1088/0964-1726/23/9/094012.

[21] S. Tomita, K. Shimanuki, K. Umemoto, A. Kawamoto, T. Nomura, and T. Tachi, "Stiff deployable structures via coupling of thick miura-ori tubes along creases," *arXiv*, vol. 2312.04048, 2023.

[22] E. T. Filipov, K. Liu, T. Tachi, M. Schenk, and G. H. Paulino, "Bar and hinge models for scalable analysis of origami," *International Journal of Solids and Structures*, vol. 124, pp. 26–45, 2017. DOI: 10.1016/j.ijsolstr.2017.05.028.

[23] K. Liu and G. H. Paulino, "Nonlinear mechanics of non-rigid origami: An efficient computational approach," *Proceedings of the Royal Society A: Mathematical, Physical and Engineering Sciences*, vol. 473, no. 2206, p. 20 170 348, 2017. DOI: 10.1098/rspa.2017.0348.

[24] J. K. Guest, J. H. Prévost, and T. Belytschko, "Achieving minimum length scale in topology optimization using nodal design variables and projection functions," *International Journal for Numerical Methods in Engineering*, vol. 61, no. 2, pp. 238–254, 2004. DOI: 10.1002/nme.1064.

[25] A. Kawamoto, T. Matsumori, S. Yamasaki, T. Nomura, T. Kondoh, and S. Nishiwaki, "Heaviside projection based topology optimization by a pde-filtered scalar function," *Structural and Multidisciplinary Optimization*, vol. 44, no. 1, pp. 19–24, 2011. DOI: 10.1007/s00158-010-0562-2.

[26] K. Svanberg, "The method of moving asymptotes—a new method for structural optimization," *International Journal for Numerical Methods in Engineering*, vol. 24, no. 2, pp. 359–373, 1987, ISSN: 0029-5981. DOI: 10.1002/nme.1620240207.